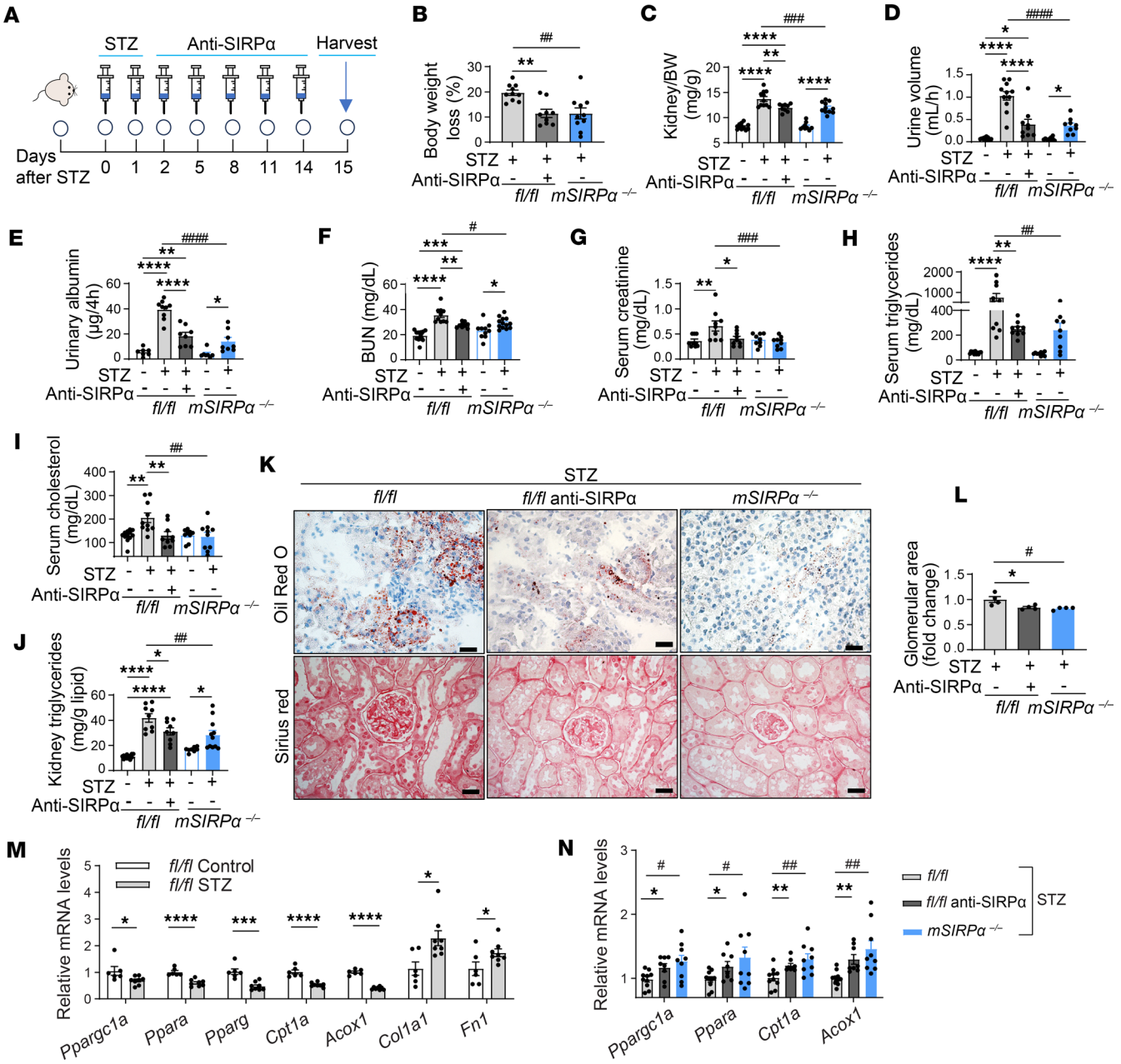

Figure 6. Blocking SIRPα in muscle attenuates streptozotocin-induced cachexia and kidney dysfunction. To induce acute diabetes, streptozotocin (STZ) was injected i.p. into *flox* (*fl/fl*) or muscle-specific SIRPα-KO (*mSIRPα*$^{-/-}$) mice, and measurements listed were made after harvest unless otherwise specified in the methods. (**A**) On day 2 after STZ injection, a group of *fl/fl* mice were given anti-SIRPα monoclonal antibody as illustrated. (**B**–**G**) Next, body weight loss (%), kidney weight, (n = 9-12), urine volume, urinary albumin, blood urea nitrogen (BUN), and serum creatinine were measured (n = 7–13). (**H** and **I**) Serum triglyceride and total cholesterol were measured (n = 9–12) after a 4 hour fast. (**J**) Kidney triglyceride to lipid weight was illustrated (n = 8-12). (**K**) Representative images of kidney lipid accumulation based on Oil red O staining and sirius red staining are shown (scale bar: 20 μm). (**L**) Glomerular area is shown (n = 4). (**M**) Relative kidney cortex mRNA levels of genes involved in fatty acid oxidation and fibrosis in control vs. STZ-treated *fl/fl* mice (n = 6–8). (**N**) Relative mRNA levels of fatty acid oxidation transcripts in kidney cortex were determined by qPCR in STZ-treated *mSIRPα*$^{-/-}$ and *fl/fl* mice ± anti-SIRPα monoclonal antibody treatment (n = 8–10). Data are shown as mean ± SEM. Statistical significance was performed using 2-tailed unpaired t test for **M** and **N**, and 1-way ANOVA followed by Bonferroni test for the rest. $^{*}P < 0.05$, $^{**}P < 0.01$, $^{***}P < 0.001$, $^{****}P < 0.0001$ Control vs. STZ or *fl/fl* STZ vs *fl/fl* STZ + anti-SIRPα; $^{\#}P < 0.05$, $^{\#\#}P < 0.01$, $^{\#\#\#}P < 0.001$, $^{\#\#\#\#}P < 0.0001$ *mSIRPα*$^{-/-}$ STZ vs. *fl/fl* STZ.

Lipid droplets, a cellular organelle specialized for storing lipids, are sometimes considered adaptive and cytoprotective against lipotoxicity (30). Although lipids are stored in lipid droplets to ensure homeostasis, ectopic lipid accumulation can be pathognomonic for DKD (31). Kang et al. reported that transgenic mice with CD36 overexpression induces kidney tubular epithelial cell lipid accumulation but that accumulation was not sufficient to induce kidney fibrosis and dysfunction (20).

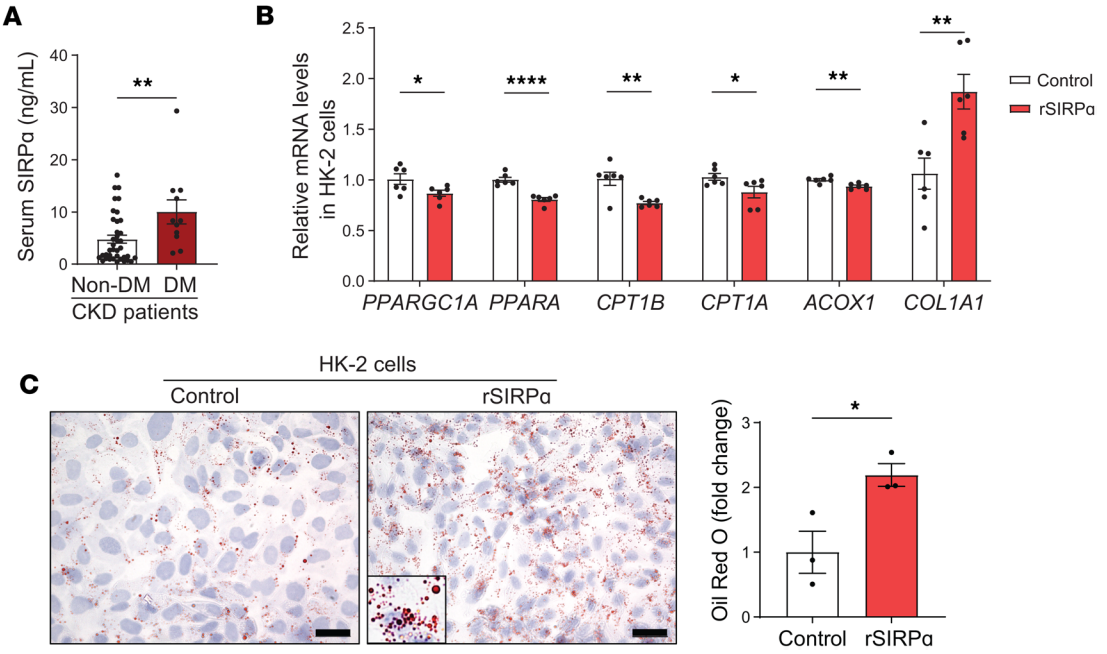

Figure 7. Type 2 diabetes stimulates circulating serum SIRPα in chronic kidney disease. (**A**) Serum SIRPα was measured in patients with type 2 diabetes mellitus (DM, $n = 11$) and non-DM ($n = 38$) patients with chronic kidney disease (CKD). (**B**) Relative mRNA levels of fatty acid oxidation transcripts and fibrosis were determined by qPCR in HK-2 cells exposed to rSIRPα treatment (500 ng/mL) for 24 hours ($n = 6$). (**C**) Lipid accumulation was determined by Oil red O staining in HK-2 cells treated with rSIRPα for 24 hours (scale bar: 25 μm, $n = 3$). Data are shown as mean ± SEM. Statistical significance was performed using 2-tailed unpaired *t* test for **A**–**C**. $^{*}P < 0.05$, $^{**}P < 0.01$, $^{****}P < 0.0001$.

Next, in control mice exposed to HFD, there is a reduction in fatty acid synthesis transcripts in kidney tissue in mice exposed to HFD (Supplemental Figure 6A) with no changes noted in fatty acid synthesis transcripts in BUMPT cells exposed to rSIRPα treatment (Supplemental Figure 6B). Additionally, rSIRPα treatment of kidney proximal tubular cells did not alter rates of fatty acid uptake (Supplemental Figure 6C). Therefore, reductions in FAO appear to contribute significantly to the dysregulation of metabolism in the obesity-induced model of diabetes. Of note, in spite of hyperglycemia and similar systolic BP, high fat–fed *mSIRPα*-KO mice displayed improved kidney FAO, with a reduction in proteinuria, and improved kidney function (reduced serum creatinine and cystatin C, important biomarkers of DKD; refs. 32, 33). Also, suppressing SIRPα in skeletal muscles or blocking the protein with anti-SIRPα monoclonal antibodies prevented STZ-induced changes in weight loss, glomerulomegaly, and kidney fibrosis, with reduced proteinuria and improved renal FAO and serum creatinine despite evidence of significant hyperglycemia. Additionally, exogenous rSIRPα exacerbated FAO and decreased ATP production, while inducing fibrosis in primary proximal tubular cells similar to hyperglycemia exposure. Additionally, fat droplets were stimulated and FAO suppressed in human proximal tubular cells exposed to rSIRPα treatment. Finally, our in vitro and in vivo data were supported by similar findings in humans, as serum SIRPα was found to be significantly higher in diabetic CKD patients compared with non-diabetic CKD patients. These results suggest a negative effect of myokine SIRPα in kidney disease. Our results are significant, as investigations in renal lipid metabolism are sparse. Specifically, renal TG accumulation has been linked to suppressed FAO expression and kidney fibrosis (20). Kidney function has long been determined based on creatinine, a muscle byproduct (7). Our results highlight the effect of dysregulation of muscle metabolism on kidney function and organ communications. Muscle secretomes including SIRPα are stimulated in response to hyperglycemia or uremic toxins (5).

In models of diabetes with hyperglycemia, suppression of muscle SIRPα improved kidney function. This is the first report to our knowledge to suggest that exogenous SIRPα directly inhibits renal tubular FAO leading to lipid accumulation in proximal tubular epithelial cells with worsening tubulointerstitial fibrosis and kidney dysfunction. The proximal tubular kidney cells share a preference for FAO as an energy source similar to cardiac muscle (6). Prior studies have elucidated the role of increasing lipid accumulation with reduced kidney FAO in DKD (20, 34, 35). These studies did not clarify specific triggers responsible for changes in FAO in renal tubular epithelial cells in DKD. Here we determined that SIRPα

independently and directly suppresses renal tubular FAO and ATP production similar to hyperglycemia. In the HFD-induced obesity model, serum SIRPα was found to be increased. Therefore, we conclude that SIRPα exerts effects on DKD to impair renal metabolic homeostasis.

Recent studies have determined that changes in kidney FAO may be a critical factor responsible for kidney dysfunction. For example, signal transducer and activator of transcription 6 (STAT6) activation leads to renal lipid accumulation with suppression of genes responsible for FAO in models of UUO or HFD (36). As well, rho-associated, coiled-coil–containing protein kinase 1 (ROCK1) has been identified a key mediator of FAO in obesity-induced diabetic nephropathy (35). Investigations into metabolic reprogramming or a shift toward a "fasting-like" process improving FA metabolism and/or utilization via SGLT2 inhibitors (SGLT2i) reveal cardio-renal protection (37, 38). Furthermore, SGLT2i may protect proximal tubular metabolic responses in favor of FAO rather than glucose metabolism while inhibiting hypoxia induced factor 1 α (HIF1α) in DKD (38). However, the effect of these studies on muscle-kidney dysfunction in DKD was not investigated. Similarly, the cardiorenal benefit associated with these treatments may be related to changes in FAO metabolism in cardiomyocytes and kidney proximal tubular cells. Future studies are needed to examine cardiac fatty acid metabolism in response to SIRPα suppression in our insulin resistant models; in addition, the timeline of muscle dysfunction and kidney disease requires further evaluation.

In conclusion, changes in muscle metabolism occur decades prior to pancreatic β cell failure or the presentation of diabetes, while exercise proves to reverse the dysregulated metabolic profile (11, 12, 39, 40). However, biomarkers for muscle metabolism are not available when these initial events occur. The importance of our study examines the influence of myokine SIRPα on kidney fatty acid metabolism. CKD is a significant independent risk factor for cardiovascular mortality; further examination is imperative in understanding how dysregulated muscle metabolism impacts kidney function. The relevance of this study details the critical role and effect of muscle on kidney function. Therefore, myokine SIRPα may serve as an important biomarker and therapeutic target in preventing DKD.

Methods

Sex as a biological variable. Our study exclusively examined male mice to limit variability in phenotype. It is unknown whether the findings in mice are relevant to female mice.

Reagents, chemicals, and antibodies. The human SIRPα ELISA kit was from LSBio (Seattle, WA). The mouse SIRPα ELISA kit was from LSBio (Shirley, MA). The mouse Cystatin C ELISA kit was obtained from Biovendor R&D (Asheville, NC). The mouse creatinine kit was from Crystal Chem (Elk Grove Village, IL). The cellular fatty acid (C16) uptake assay kit was from Cayman (Ann Arbor, MI). BUN measurements were illustrated by Roman et al. (41). Picrosirius Red Stain Kit was obtained from Polysciences (Warrington, PA). Clarity Urocheck 2 GP Test Strips (Boca Raton, FL) were used for urine glucose measurements. The mouse Albumin ELISA kit was from Crystal Chem (Elk Grove Village, IL). The RNeasy Fibrous Tissue Mini Kit and RNase-Free DNase Set were from Qiagen (Valencia, CA); iScript cDNA Synthesis Kit and iQ SYBR Green Supermix were from Bio-Rad (Hercules, CA). HIScript III RT SuperMix for qPCR (+gDNA wiper) was from Vazyme (Nanjing, China) for the cDNA synthesis of BUMPT cell. The phosphatase inhibitor and protease inhibitor were from Roche (Indianapolis, IN). TRIzol was from Life Technologies (Carlsbad, CA); RIPA lysis and extraction buffer was from G-Biosciences (St. Louis, MO). STZ and insulin were from Sigma Aldrich (St. Louis, MO). The human renal proximal tubular cell line HK-2 from ATCC (Manassas, VA) was cultured in Keratinocyte SFM (1X) media with human recombinant epidermal growth factor (rEGF), bovine pituitary extract (BPE) supplement and fetal bovine serum (FBS) (Gibco, USA). The antibody against GAPDH (Cat. No. MA5-15738) was from Invitrogen (Rockford, IL). SIRPα (Cat. No. 13379), p-AKT (S473, Cat. No. 4060), AKT (Cat. No. 2920), UCP1 (Cat. No. 14670), and TSP1 (Cat. No. 37879) were from Cell Signaling Technology (Beverly, MA). Fibronectin (Cat. No. F3648) and αSMA (Cat. No. A5228) were from Sigma Aldrich (St. Louis, MO). InvivoMAb anti-mouse SIRPα P84 (Cat. No. BE0322) monoclonal antibody was from Bio X Cell (Lebanon, NH).

Animals. We studied skeletal muscle-specific SIRPα (*mSIRPα*$^{-/-}$) KO mice or *flox* mice (*SIRPα*$^{fl/fl}$ or *fl/fl*), which were housed in 12-hour light/dark cycles (6 a.m. to 6 p.m.) at 24°C and fed ad libitum either a standard rodent chow or HFD (60%). *SIRPα*$^{fl/fl}$ mice were obtained in conjunction with the BaSH EUCOMM; *mSIRPα*$^{-/-}$ were created with deletion of exons 3 and 4 were generated using Cre (muscle creatine kinase-Cre) mice from The Jackson Laboratory (Bar Harbor, ME) recombinase:loxP system as described previously (6). These genetically modified mice are on *C57BL/6* background with a grossly normal phenotype.

HFD model. *SIRPα*$^{fl/fl}$ or *mSIRPα*$^{-/-}$ male mice at 5 weeks of age were randomly allocated to 2 groups: (a) NC with 15% of calories from fat (Cat. No. PicoLab 5V5R, LabDiet, Richmond, IN) or (b) HFD with 60% of calories from fat (Cat. No. D12492, Research Diets, New Brunswick, NJ). The mice were fed with the NC or HFD for 16 weeks. Sixteen-hour fasting serum was used to check serum insulin levels. Random-feeding serum was used to check blood creatinine and cystatin C after 16 weeks of HFD. Urine was collected for 24 hours and used to check albumin and glucose levels after 14 weeks of HFD. For *SIRPα*$^{fl/fl}$ and *mSIRPα*$^{-/-}$ mice, GTT was performed at 9 and 14 weeks; ITT was performed at 11 and 13 weeks using an Advanced Glucose Meter (Woonsocket, RI). For GTT, 16-hour fasted mice were injected i.p. with 1.5 g/kg glucose, and tail vein blood was evaluated at 0-, 30-, 60-, 90-, and 120-minute intervals. For ITT, 5-hour fasted mice were injected i.p. with 1.5 units/kg insulin, and tail vein blood was evaluated at 0-, 15-, 30-, 60-, 90-, and 120-minute intervals to measure blood glucose concentration.

Whole-body energy metabolism test/ indirect calorimetry. After 10 weeks on HFD, whole-body energy metabolism of the mice was assessed in the metabolic cages using a Comprehensive Lab Animal Monitoring System (CLAMS, Columbus Instruments, Columbus, OH) in the Mouse Phenotyping Core at BCM. CLAMS cages were housed in temperature-controlled environmental chambers at 23°C on a standard 12-hour light/dark cycles. Animals were monitored for 48 h, and during that time, food and water were provided ad libitum. Parameters monitored include VO_2, VCO_2, respiratory exchange ratio (RER), heat, physical activity, and food/water consumption.

Grip strength. Forelimb grip strength was assessed after 14 weeks in *SIRPα*$^{fl/fl}$ and *mSIRPα*$^{-/-}$ mice on NC or HFD. Each mouse was pulled backward in a straight, horizontal line to display peak force obtained by Grip Strength Meter (Columbus Instruments, Columbus, OH). Grip strength was measured greater than 3 times for each mouse and the average measurement was illustrated.

BP measurements. After 16 weeks of HFD, a noninvasive tail-cuff system (BP-2000, Visitech Systems, Apex, NC) was used to measure indirect BP and heart rate for conscious nonanesthetized mice.

STZ model. For acute diabetes, 3-month-old *SIRPα*$^{fl/fl}$ and *mSIRPα*$^{-/-}$ male mice were fasted overnight and administered 150 mg/kg/day 2 days STZ i.p. Food was immediately provided after injections. Mice were monitored for hyperglycemia. The blood glucose reached 373 ± 31 mg/dL 2 days after injection and reached 533 ± 18 mg/dL 1 week after injection and 588 ± 7 mg/dL 2 weeks after STZ infection. On day 2, *SIRPα*$^{fl/fl}$ mice were injected with 200 μg of anti-SIRPα monoclonal antibody or control mice received diluent i.p. every 72 hours for a total of 5 doses before harvest. Mice were fed a NC diet during the experiment. Four-hour fasting serum was used to check BUN, TG, and cholesterol on day 13. Four-hour collection of urine with random feeding was used to check urine volume and albumin on day 14. After harvest on day 15, organ weight, gene transcripts, kidney slides, and serum (filtered by Pierce Spin Columns, Thermo Scientific, Rockford, IL) creatinine were analyzed.

Proximal tubular cells and in vitro treatment. Mouse proximal tubular cells were collected from 12-week-old *SIRPα*$^{fl/fl}$ mice fed with NC referred to Peng et al. (9). Mice were euthanized and kidneys were collected in a septic environment. Kidney cortices were dissected visually, minced into small pieces, and digested in 5 mL 37°C preheated DMEM medium containing 2 mg/mL type I collagenase and 1% HEPES (Lonza, Walkersville, MD), then placed into a shaking incubator at 37°C and 5% CO_2 for 30 minutes. The filtered tissue suspension was collected by a 100 μm strainer (Tisch Scientific, Cleves, OH). Then the samples were centrifuged at 53*g* for 2 minutes to pellet the kidney tubules, washed with DMEM containing 10% FBS and then centrifuged again at 53*g*. The final pellet, consisting mostly of renal tubules, was resuspended in 25 mM glucose DMEM medium supplemented with 10% (v/v) FBS and 1% penicillin-streptomycin (Gibco, USA) and plated in cell culture treated dish and thus these cultured cells were not polarized.

BUMPT cells (the mouse proximal tubule–derived cell line) (in house) were directly seeded in cell culture treated dish with 25 mM glucose DMEM medium containing 10% (v/v) FBS and 1% penicillin-streptomycin at 37°C in 5% CO_2 to reach 30%–40% confluence by the next day. When the cell confluency reached 80%, they were used for treatment. For high glucose treatment, BUMPT cells were treated with 6 or 24-hour high glucose (75 mM) and compared with standard glucose media (25 mM). For low glucose treatment, BUMPT cells were treated with 6 or 24-hour low glucose (5.5 mM) and compared with standard glucose media (25 mM). BUMPT cells treated with different concentrations of glucose were used to test the cell energy metabolism by the Seahorse XFe96 analyzer (Agilent Technologies, Santa Clara, CA).

Mouse SIRPα recombinant protein (115-125 kDa on SDS-PAGE gel in reducing conditions) was commercially made from the mouse myeloma cell line NS0 (R&D Systems, Minneapolis, MN), specifically not a full-length protein but includes amino acid sequences from Met1-Asn373 in the N-terminus. Human SIRPα recombinant protein (70–105 kDa on SDS-PAGE gel in reducing conditions) was commercially made from Chinese Hamster Ovary (CHO) cell line (R&D Systems, Minneapolis, MN), specifically not a full-length protein but includes amino acid sequences Gly27-Arg370 in the N-terminus. For mouse recombinant SIRPα (rSIRPα) treatment, 500 ng/mL rSIRPα was directly added, without filter, to the media of primary proximal tubular kidney cells or BUMPT cells for 6 h, 24 h, 48 h or 72 h. Cell energy metabolism of BUMPT cells treated with rSIRPα was evaluated by the Seahorse XFe96 analyzer. Fatty acid uptake measurements were made in BUMPT cells treated with or without rSIRPα utilizing Cellular Fatty Acid (C16) Uptake Assay Kit (Cayman, Ann Arbor, MI). Cells were starved for 1 hour in serum-free cultured media and incubated for 1 hour with 500 ng/mL rSIRPα or vehicle control, after which BODIPY-palmitate working solution was added. Negative controls utilized did not contain BODIPY-palmitate. Kinetic measurements of palmitate fatty acid uptake were made every 5 minutes for up to 60 minutes.

Human kidney proximal tubular HK-2 cells from ATCC (Manassas, VA) were cultured in Keratinocyte Serum Free Medium (K-SFM) with supplement of 0.05 mg/mL bovine pituitary extract (BPE), 5 ng/mL human recombinant epidermal growth factor (EGF), 10% FBS and 1% penicillin-streptomycin. HK-2 cells at 80% confluency were exposed to human rSIRPα (500 ng/mL) for 24 h. At the end of incubation, cellular protein was extracted and stored at –80°C.

Section and staining. For H&E and sirius red staining, tissue sections (6 μm) were fixed in 4% paraformaldehyde, embedded in paraffin. The myofiber sizes of TA were obtained using NIS-Elements Br 3.0 software (Nikon Instruments, Melville, NY). Frozen cryosections (8 μm) of kidney from STZ mice were mounted on glass slides. For Oil red O (ORO) staining, kidney tissues or cell cultures were fixed in 4% paraformaldehyde for 2 or 30 minutes, respectively, at room temperature, and the slides were stained with a 0.2% Oil red O solution for 15 minutes. Kidney fibrosis was checked by Picrosirius Red Stain Kit. Images were processed using a Nikon 80i microscope (Nikon Instruments, Melville, NY). The experimenter/analyzer was blinded to the treatment groups.

Western blots. We homogenized 30 mg kidney/muscle tissue or 100 mg fat tissue for 1 min in 300 μL cold RIPA buffer supplemented with protease and phosphatase inhibitor cocktails. The homogenates were incubated on ice for 10 minutes and then centrifuged (15,600*g*) at 4°C for 15 minutes. The supernatants were used as whole cell lysates. Protein concentration was determined by Pierce BCA Protein Assay (Thermo Scientific, Rockford, IL). An equal amount of protein (80-100 μg) was separated on sodium dodecyl sulfate- polyacrylamide gel electrophoresis in tris/glycine buffer, transferred to nitrocellulose blotting membrane, blocked for 20 minutes, and blotted with all primary antibodies diluted (1:1,000) except fibronectin (1:3,000) in blocking buffer overnight at 4°C. After 3 times of washing in TBS containing 0.1% Tween20, the membrane was incubated in secondary antibody diluted with TBS containing 0.1% Tween20 for 1 hour and washed mentioned earlier above, and the protein was detected using the ChemiDoc MP Imaging System (Bio-Rad, Hercules, CA). The protein of interest was analyzed using Image Lab 6.0 (Bio-Rad, Hercules, CA), and the protein intensities were quantified using NIH ImageJ software. GAPDH was used as an internal standard unless otherwise specified to quantify Western blot bands.

qPCR. Total RNA of tissue or cells was extracted using TRIzol. First-strand cDNA was synthesized from 1 μg DNase-treated total RNA using Reverse Transcription Supermix for qPCR. The mRNA levels were evaluated by qPCR using SYBR Green Supermix. Reactions of qPCR were performed in 96-well format using a CFX96 Real-Time System (Bio-Rad, Hercules, CA). The reaction volume was 10 μL, including 5 μL SYBR Green Supermix, 2 μL 2.5 μm primer, and 1 μL cDNA. The following thermal cycling profile was used: 95°C 3 minutes before 40 cycles of 95°C for 15 seconds and 60°C for 30 seconds, followed by 55°C–95°C increment for dissociation curve analysis. The relative mRNA levels were calculated using the comparative $2^{-\Delta\Delta CT}$ Method (Livak and Schmittgen, 2001) and normalized to *Gapdh* or *Rn18s* (kidney FAO transcripts).

Primer sequences. Primer sequences of mouse genes include the following: *Gapdh* F: 5′-TGTGATGGGTGTGAACCACGAGAA-3′, R: 5′-CATGAGCCCTTCCACAATGCCAAA-3′; *Rn18s* F: 5′-GTAACCCGTTGAACCCCATT-3′, R: 5′-CCATCCAATCGGTAGTAGCG-3′; *Ppargc1a* F: 5′-TCCTCTTCAAGATCCTGTTAC-3′, R: 5′-CACATACAAGGGAGAATTGC-3′; *Ppara* F: 5′-GAATCCACGAAGCCTACC-3′, R: 5′-GCCATACACAAGGTCTCC-3′; *Pparg* F: 5′-GCGGTGAACCACTGATAT-3′, R: 5′-TGGCATCTCTGTGTCAAC-3′; *Acox1* F: 5′-CAGAGTTAATCACGCACATC-3′, R: 5′-TGGATCGTTCAGAATCAAGT-3′; *Cpt1a* F: 5′-GGTCTTCTCGGGTCGAAAGC-3′, R: 5′-TCCTCCCACCAGTCACTCAC-3′;

Fasn F: 5′-GAGCCCAGACAGAGAAGA-3′, R: 5′-GTCCACACCACCAATGAG-3′; *Acaca* F: 5′-ATTGGGCACCCCAGAGCTA-3′, R: 5′-CCCGCTCCTTCAACTTGCT-3′; *Srebf1* F: 5′-AATAAATCTGCTGTCTTGCG-3′, R: 5′-CCTTCAGTGATTTGCTTTTG-3′; *Il6* F: 5′-AGCCAGAGTCCTTCAGAGAGA-3′, R: 5′-TAGGAGAGCATTGGAAATTGGG-3′; *Tnf* F: 5′-CATGAGCACAGAAAGCATGATCCG-3′, R: 5′-AAGCAGGAATGAGAAGAGGCTGAG-3′; *Trim63* F: 5′-GTGTGAGGTGCCTACTTGCTC-3′, R: 5′-GCTCAGTCTTCTGTCCTTGGA-3′; *Fbxo32* F: 5′-CTGAAAGTTCTTGAAGACCAG-3′, R: 5′-GTGTGCATAAGGATGTGTAG-3′; *Fn1* F: 5′-AATCGTGCAGCCTCAATC-3′, R: 5′-CCTCCATAGCAGGTACAAAC-3′; *Col1a1* F: 5′-GTTCAGCTTTGTGGACCTC-3′, R: 5′-GGCAGATACAGATCAAGCAT-3′; *Lep* F: 5′-CTTTGGTCCTATCTGTCTTATG-3′, R: 5′-TCTTGGACAAACTCAGAATG-3′; *Adipoq* F: 5′-CCACTTTCTCCTCATTTCTG-3′, R: 5′-CTAGCTCTTCAGTTGTAGTAAC-3′.

Human genes. Primer sequences of human genes include the following: *GAPDH* F: 5′-CTTTTGCGTCGCCAG-3′, R: 5′-TTGATGGCAACAATATCCAC-3′; *PPARGC1A* F: 5′-GCAGACCTAGATTCAAACTC-3′, R: 5′-CATCCCTCTGTCATCCTC-3′; *PPARA* F: 5′-CCTAAAAAGCCTAAGGAAACC-3′, R: 5′-GATCTCCACAGCAAATGATAG-3′; *CPT1A* F: 5′-ACGGGGATTATAAGTCAAGG-3′, R: 5′-CACAGCAAGTGAAAATCAAC-3′; *CPT1B* F: 5′-AGAATTCCAGGACAAGACTG-3′, R: 5′-CACTCACATAGTTACTTGCC-3′; *ACOX1* F: 5′-AAAGCAGAGGTCCACG-3′, R: 5′-CCACAAAATTTGAGTTGCAC-3′; *COL1A1* F: GCTATGATGAGAAATCAACCG-3′, R: 5′-TCATCTCCATTCTTTCCAGG-3′.

Statistics. Values are expressed as mean ± SEM. Significance analysis was performed using 2-tailed unpaired Student's *t* test to compare data between 2 groups and 1-way ANOVA followed by Bonferroni for multiple variables unless otherwise specified in the figure legends. $P < 0.05$ was considered statistically significant. GraphPad Prism software was used for statistical analysis.

Study approval. All animal procedures were performed in accordance with the standards set forth in the guidelines for IACUC of BCM.

The procedures for human samples were approved by the Ethics Committee of the Department of Internal Medicine of the University of Genoa, in accordance with the Declaration of Helsinki regarding ethics of human research. Serum samples were obtained from patients with advanced kidney disease. Before the patients' participation, the nature, purpose, and risks of the study were reviewed with all the participants, and their voluntary consent was obtained. The detailed characteristics of patients with CKD are available in Supplemental Table 1.

Data availability. All data associated with this study are present in the paper or the supplemental information, and raw data are included in the Supporting Data Values file.

Author contributions

SST and JW carried out experiments, study design, figure legends, and data analysis. DSH, QL, and ZH contributed to experiments related to the Seahorse experiment. ER and DV contributed to sample collection and measurements. JW, BK, and HZ contributed to histological examination, while WEM contributed to editing. SST, the principal investigator, conceptualized the study, obtained funding, and drafted the manuscript. All the authors reviewed, contributed to, and approved the final manuscript.

Funding support

- VA Merit Award 1I01BX005792 to SST from the United States Department of Veterans Affairs, Biomedical Laboratory Research and Development Program.
- 2I01BX002006 to DSH from the United States Department of Veterans Affairs, Biomedical Laboratory Research and Development Program.
- American Society of Nephrology Carl W. Gottschalk Research Scholar Grant to SST.
- Baylor College of Medicine MMPC, funded by NIH RO1DK114356 & UM1HG006348.

Acknowledgments

We acknowledge the generous support of Dr. and Mrs. Harold Selzman.

Address correspondence to: Sandhya S. Thomas, Selzman Institute for Kidney Health, Department of Medicine-Nephrology, Baylor College of Medicine, BCM 395, Houston, Texas 77030, USA. Phone: 713.798.2402; Email: ssthomas@bcm.edu.

1. Gonzalez-Rocha A, et al. Risk prediction score for chronic kidney disease in healthy adults and adults with type 2 diabetes: systematic review. *Prev Chronic Dis*. 2023;20:E30.
2. Koye DN, et al. The global epidemiology of diabetes and kidney disease. *Adv Chronic Kidney Dis*. 2018;25(2):121–132.
3. Fliser D, et al. Insulin resistance and hyperinsulinemia are already present in patients with incipient renal disease. *Kidney Int*. 1998;53(5):1343–1347.
4. Thomas SS, et al. Signal regulatory protein-α interacts with the insulin receptor contributing to muscle wasting in chronic kidney disease. *Kidney Int*. 2013;84(2):308–316.
5. Thomas SS, et al. SIRPα mediates IGF1 receptor in cardiomyopathy induced by chronic kidney disease. *Circ Res*. 2022;131(3):207–221.
6. Wu J, et al. Signal regulatory protein alpha initiates cachexia through muscle to adipose tissue crosstalk. *J Cachexia Sarcopenia Muscle*. 2019;10(6):1210–1227.
7. Patel SS, et al. Serum creatinine as a marker of muscle mass in chronic kidney disease: results of a cross-sectional study and review of literature. *J Cachexia Sarcopenia Muscle*. 2013;4(1):19–29.
8. Verzola D, et al. Enhanced myostatin expression and signalling promote tubulointerstitial inflammation in diabetic nephropathy. *Sci Rep*. 2020;10(1):6343.
9. Peng H, et al. Myokine mediated muscle-kidney crosstalk suppresses metabolic reprogramming and fibrosis in damaged kidneys. *Nat Commun*. 2017;8(1):1493.
10. Hanatani S, et al. Akt1-mediated fast/glycolytic skeletal muscle growth attenuates renal damage in experimental kidney disease. *J Am Soc Nephrol*. 2014;25(12):2800–2811.
11. Kosmadakis GC, et al. Benefits of regular walking exercise in advanced pre-dialysis chronic kidney disease. *Nephrol Dial Transplant*. 2012;27(3):997–1004.
12. Mustata S, et al. Effects of exercise training on physical impairment, arterial stiffness and health-related quality of life in patients with chronic kidney disease: a pilot study. *Int Urol Nephrol*. 2011;43(4):1133–1141.
13. Traise A, et al. The effect of exercise training in people with pre-dialysis chronic kidney disease: a systematic review with meta-analysis. *J Nephrol*. 2024;37(8):2063–2098.
14. Shurraw S, et al. Association between glycemic control and adverse outcomes in people with diabetes mellitus and chronic kidney disease: a population-based cohort study. *Arch Intern Med*. 2011;171(21):1920–1927.
15. Action to Control Cardiovascular Risk in Diabetes Study Group, et al. Effects of intensive glucose lowering in type 2 diabetes. *N Engl J Med*. 2008;358(24):2545–2559.
16. Afshinnia F, et al. Increased lipogenesis and impaired β-oxidation predict type 2 diabetic kidney disease progression in American Indians. *JCI Insight*. 2019;4(21):e130317.
17. Bhargava P, Schnellmann RG. Mitochondrial energetics in the kidney. *Nat Rev Nephrol*. 2017;13(10):629–646.
18. Pagliarini DJ, et al. A mitochondrial protein compendium elucidates complex I disease biology. *Cell*. 2008;134(1):112–123.
19. Rinaldi A, et al. Impaired fatty acid metabolism perpetuates lipotoxicity along the transition to chronic kidney injury. *JCI Insight*. 2022;7(18):e161783.
20. Kang HM, et al. Defective fatty acid oxidation in renal tubular epithelial cells has a key role in kidney fibrosis development. *Nat Med*. 2015;21(1):37–46.
21. Brouwers B, et al. Phlorizin pretreatment reduces acute renal toxicity in a mouse model for diabetic nephropathy. *J Biol Chem*. 2013;288(38):27200–27207.
22. Hirai H, et al. Leishmania infection-induced proteolytic processing of SIRPα in macrophages. *Pathogens*. 2023;12(4):593.
23. Vladimirova YV, et al. A new serum macrophage checkpoint biomarker for innate immunotherapy: soluble signal-regulatory protein alpha (sSIRPα). *Biomolecules*. 2022;12(7):937.
24. Cara-Fuentes G, et al. Pulmonary surfactants and the respiratory-renal connection in steroid-sensitive nephrotic syndrome of childhood. *iScience*. 2022;25(8):104694.
25. Kolb H, et al. Insulin translates unfavourable lifestyle into obesity. *BMC Med*. 2018;16(1):232.
26. Kloting N, et al. Insulin-sensitive obesity. *Am J Physiol Endocrinol Metab*. 2010;299(3):E506–E515.
27. Severinsen MCK, Pedersen BK. Muscle-organ crosstalk: the emerging roles of myokines. *Endocr Rev*. 2020;41(4):594–609.
28. Ma S, et al. Skeletal muscle-derived extracellular vesicles transport glycolytic enzymes to mediate muscle-to-bone crosstalk. *Cell Metab*. 2023;35(11):2028–2043.
29. Baar K, et al. Adaptations of skeletal muscle to exercise: rapid increase in the transcriptional coactivator PGC-1. *FASEB J*. 2002;16(14):1879–1886.
30. Pressly JD, et al. Adaptive and maladaptive roles of lipid droplets in health and disease. *Am J Physiol Cell Physiol*. 2022;322(3):C468–C481.
31. Mitrofanova A, et al. Kidney lipid dysmetabolism and lipid droplet accumulation in chronic kidney disease. *Nat Rev Nephrol*. 2023;19(10):629–645.
32. Mussap M, et al. Cystatin C is a more sensitive marker than creatinine for the estimation of GFR in type 2 diabetic patients. *Kidney Int*. 2002;61(4):1453–1461.
33. Sapkota S, et al. Diagnostic accuracy of serum cystatin C for early recognition of nephropathy in type 2 diabetes mellitus. *Int J Nephrol*. 2021;2021:8884126.
34. Herman-Edelstein M, et al. Altered renal lipid metabolism and renal lipid accumulation in human diabetic nephropathy. *J Lipid Res*. 2014;55(3):561–572.
35. Nagai Y, et al. Rho-associated, coiled-coil-containing protein kinase 1 regulates development of diabetic kidney disease via modulation of fatty acid metabolism. *Kidney Int*. 2022;102(3):536–545.
36. Li J, et al. STAT6 contributes to renal fibrosis by modulating PPARα-mediated tubular fatty acid oxidation. *Cell Death Dis*. 2022;13(1):66.
37. Gao YM, et al. Cardiorenal protection of SGLT2 inhibitors-perspectives from metabolic reprogramming. *EBioMedicine*. 2022;83:104215.

38. Cai T, et al. Sodium-glucose cotransporter 2 inhibition suppresses HIF-1α-mediated metabolic switch from lipid oxidation to glycolysis in kidney tubule cells of diabetic mice. *Cell Death Dis*. 2020;11(5):390.
39. Bishop NC, et al. Exercise and chronic kidney disease: potential mechanisms underlying the physiological benefits. *Nat Rev Nephrol*. 2023;19(4):244–256.
40. DeFronzo RA, Tripathy D. Skeletal muscle insulin resistance is the primary defect in type 2 diabetes. *Diabetes Care*. 2009;32 Suppl 2(suppl 2):S157–S163.
41. Roman RJ, et al. Fluorometric assay for urea in urine, plasma, and tubular fluid. *Anal Biochem*. 1979;98(1):136–141.